RESEARCH ARTICLE

Frontiers in Advanced Materials Research

DOI: 10.34256/famr1913

Cytocompatibility and Dielectric Properties of Sr^{2+} Substituted Nano-Hydroxyapatite for Triggered Drug Release

Lakshmanaperumal Sundarabharathi [a,*], Mahendran Chinnaswamy [a], Hemalatha Parangusan [b], Deepalekshmi Ponnamma [b], Mariam Al Ali Al-Maadeed [c]

[a] Department of Physics, Sri Ramakrishna Mission Vidyalaya College of Arts and Science, Coimbatore 641 020, Tamilnadu, India.

[b] Center for Advanced Materials, Qatar University, P. O. Box 2713, Doha, Qatar

[c].

*Corresponding Author
lakshmanphd1201@gmail.com
(L. Sundarabharathi)

Received : 31st January 2019
Accepted : 4th March 2019

ABSTRACT: Hydroxyapatite ($Ca_5(PO_4)_3OH$) is a well-known bioceramics material used in medical applications because of its ability to form direct chemical bonds with living tissues. In this context, we investigate the biocompatibility and dielectric properties of Sr2+-substituted hydroxyapatite nanoparticles were synthesized by sol-gel method. The influence of strontium on the crystal structure, functional group, morphological, electrical properties, and biocompatibility of as-synthesized nano-hydroxyapatite samples was analyzed using X-ray diffraction (XRD), Fourier transform infrared (FTIR) spectroscopy and field emission scanning electron microscopy (FE-SEM). Dielectrical properties of the bioactive Sr-HA sample were investigated by a dielectric impedance spectroscopy method. The observed results illustrate the incorporation of Sr2+ ions in the apatite lattice could influence the pure HA properties, by reducing the crystallite size and crystallinity quite consistent with the morphology variation. The ac conductivity (σ_{ac}) increased with an increasing applied frequency confirmed that prepared HA sample exhibited the universal power law nature. Further, the in vitro drug loading and release studies using doxycycline as a model drug demonstrate that the Sr2+ -HA nanoparticles show high drug adsorption capacity and sustained drug release. Thus, the improved bioceramics system could be a promising candidate for future biomedical applications.

Keywords: Hydroxyapatite, Sol-gel, doxycycline, Biocompatibility, Bone Implant

1. Introduction

Bioactive nanomaterials have more attention for their use in specific clinical applications. In particularly, the synthetic bioactive nanomaterials to repair and reconstruction of hard tissues has appreciably employed in the past years [1, 2]. Hydroxyapatite ($Ca_{10}(PO_4)_6(OH)_2$, HA) is most eminent bioceramic material since it is chemical and structural similarity to the mineralized constituent of hard tissues. This biomaterial attributes infer good biocompatibility and osteoconductivity [3]. However, synthetic HA varies significantly from other bioactive material due to its crystallinity, composition, less reactivity with bone, inferior osteogenic capacity and poor mechanical strength [4]. In order to ionic substitution convenience way to tailoring their characteristic properties of synthetic HA and overcomes the relative drawbacks [5]. The inclusion of well biological desirable ions with HA could be an increase in bone mineral density and it is direct to use in bone implant. Natural human bone contains several trace elements such as Mg^{2+}, Sr^{2+}, Zn^{2+} and F^- which play an important role in enhance osteoconductivity and mechanical strength of bone [6]. Among the divalent cations, Sr^{2+} is particularly attractive due to beneficial effects in the treatment of osteoporosis. Incorporation of strontium into HA lattice can leads to favorable effects on biomaterial properties, such as change in crystallinity, solubility in chemical solvents, and dissolution which may in turn influence on bioactive property [3]. In addition, *in vitro* and *in vivo* study has been deals with the Sr^{2+} enhances bone formation and reduces bone loss which expecting leads to a increase in bone mineral density and improved bone strength [7].

Taken together, strontium containing tooth paste was developed to increase the remineralization of dental enamel. Thus many efforts have been made to improve the bioactivity and biocompatibility of Sr-substituted HA [8]. Frasnelli et al. [9] strontium-substituted hydroxyapatite nanoparticles could be potentially used to bone tissue and tissue regeneration. Suganthi et al. [10] highlighted the fibrous growth of Sr

substituted HA increased the surface area leading to the prolonged release of drug compared to pure HA. *In vitro* and *in vivo* studies revealed the inclusion of Sr into HA structure increases bone forming ability and improved bone strength for human hard tissues [4]. Hence, Sr^{2+} is an appreciably and topical ion for substitution into HA due to its important role in the biomineralization of hard tissues. Several synthetic methods employed to generate hydroxyapatite nanoparticles such as microwave assisted, hydrothermal, sol-gel, solvothermal, and high-gravity precipitation methods. Among theses, the Sol-gel method extends eminent advantages including high phase purity, homogenous mixture, and low synthesis temperature [11-14]. The major aim of this work to synthesize lower amount of Sr^{2+}-substituted HA nanoparticles using sol-gel method. The influence of Sr^{2+} ions incorporation on crystal structure, morphology, dielectric properties and drug release of HA nanoparticles were investigated. Biocompatibility was carried out using human lung adenocarcinoma epithelial cells (A549) to estimate the cytotoxicity of the Sr^{2+}-substituted HA nanoparticles.

2. Materials and Method

2.1. Source Materials

The starting chemicals used in this experiment were of analytical grade without further any purification. Calcium nitrate tetrahydrate ($Ca(NO_3)_2.4H_2O$, 98.0 % purity, Merck), diammonium hydrogen phosphate ($(NH_4)_2HPO_4$, 99% purity, Merck), strontium nitrate hexahydrate ($Sr(NO_3)_2.6H_2O$, 98% purity, Sigma-Aldrich), sodium hydroxide (NaOH, 98% purity, Sigma-Aldrich) pellets, ($C_{10}H_{16}N_2O_8$, 98% purity, LobaChemie) were obtained commercially. Millipore water was used as the solvent throughout the experiments.

2.2. Sample Preparation

In briefly, specific quantities of source materials Ca^{2+} and Sr^{2+} mixed in millipore water to form solution A and the total amount of Ca^{2+} and Sr^{2+}in 0.5 M. 0.3 M of diammonium hydrogen phosphate were dissolved in millipore water to form solution B. The Ca^{+} dopant: P molar ratio was adjusted at 1.67. Then, solution B was added dropwise into solution A with vigorous stirring for 1 h at room temperature. The ammonia solution was used to maintain the pH value at 10. After the addition, the milky solution was observed and kept at 90 °C for overnight. Subsequently, the attained precipitate was filtered off and washed several times with millipore water and ethanol. The resulting white gel was dried at 120 °C for about 14 h in hot air oven. Finally, the derived white powders were calcined at 700 °C for 2 h heating rate at 20 °C min^{-1}.The reaction for the formation of Sr-substituted HA is expressed as follows:

$$(10-x)Ca^{2+} + x\,Sr^{2+} + 6PO^{3-}{}_4 + 2OH^- \rightarrow Ca_{10-x}Sr_x(PO_4)_6\,(OH)_2$$

2.3. Characterization techniques

Crystal structure of the as-synthesized HA nanoparticles were of characterized by Bruker D8 Advance X-ray diffractometer (XRD) equipped with Cu Kα radiation (λ=1.542 Å). Fourier transform Infrared (FT-IR) spectra are recorded in the wave number range of 4000–400 cm^{-1} using a Nicolet 380 spectrometer. The surface morphology was analyzed using field emission scanning electron microscope (FESEM, Zeiss, 6027 Merlin compact). The dielectric and alternating current conductivity properties were examined by using a Hioki 3532-50 LCR Hi Tester at room temperature.

2.3.1. *In vitro* drug release

To examine the *in vitro* drug release, Amoxicillin was used to selected model drug in this study [15]. 10 mg of as-synthesized HA nanoparticles were mixed with 5 mg of amoxicillin and made it into a pellet. The pellet immersed in PBS solution was kept maintained at room temperature. The release medium was drawn at appropriate time intervals and the amount of drug released was calculated by UV- Vis spectrophotometer (Shimadzu, UV 3600) at 230 nm.

2.3.2. *In vitro* Cytotoxicity

The human lung carcinoma epithelial- A549 cell line were grown in eagles minimum essential medium containing 10% fetal bovine serum (FBS). The cell culture was maintained in a humidity atmosphere at 37 °C, with 5% CO_2 and 95% air and the culture medium was changed twice a week. To evaluate the cytotoxicity of the prepared sample at different concentrations, Viable cells were counted by using a hemocytometer and diluted with medium containing 5% FBS to give a final density of $1x10^5$ cells/mL in a humidified atmosphere. The medium with MTT solution was discarded, the addition of DMSO (100 µL) and the plate was shaken for 10 min before measuring absorbance at 570 nm using photometer. The cell viability in % was determined using the following formula [6],

$$Cell\ Viability\ \% = \frac{Test}{Control} X100 \qquad [1]$$

3. Results and discussion

3.1. XRD Analysis

The X-ray powder diffraction patterns of the pure HA and Sr-substituted HA nanoparticles are shown in Fig.1. The major diffraction peaks correspond to the (002), (102), (211), (112), (300), (202), (301), (113), (203), (222) (213) and (004) crystal planes are obviously in good agreement with the standard JCPDS reference (01–084) and the secondary phase of β-tricalciumphosphate (β-TCP) (09–0169) appears in both samples. All the diffraction peaks are well indexed as pure hexagonal phase structure, and no discernable peaks of third phase are found. The sharp diffraction peaks manifests that the pure and Sr-HA samples have good crystalline nature. However, for the Sr substituted HA sample, the diffraction peaks exhibited a slight increase

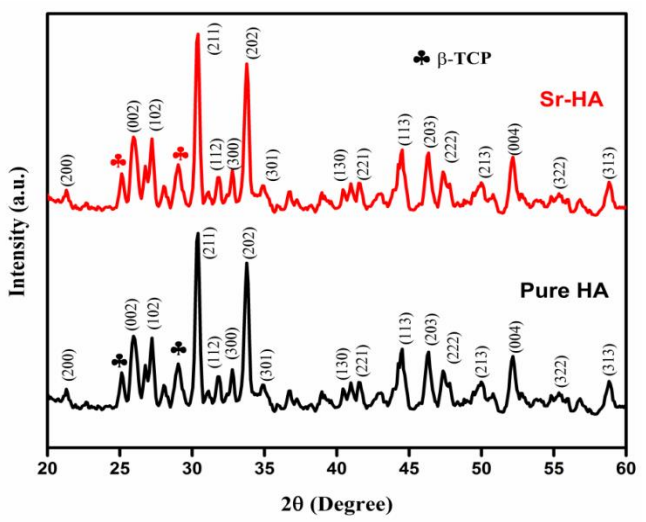

Fig. 1. XRD patterns of Pure and Sr-substituted HA nanoparticles by Sol-gel method.

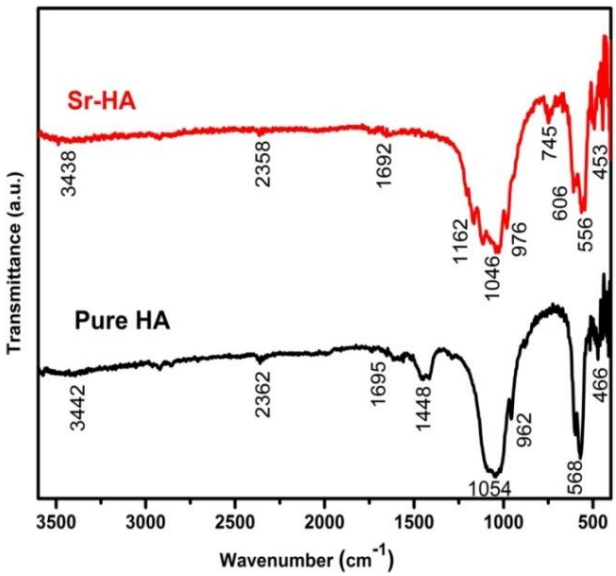

Fig. 2. FTIR spectra of pure and Sr^{2+}substituted HA nanoparticles.

In peak width, which indicating the decreased crystallinity and crystallite size.

The peak broadening relates to crystallite size (D) according to the following Scherrer's Equation [2],

$$D = \frac{0.9\lambda}{\beta cos\Theta} \qquad [2]$$

Where λ is the wavelength of the X-ray (λ=0.154 nm), Θ is the diffraction angle in degree and β is the full-width at half maximum (FWHM) in radian. By pure HA and Sr-substituted HA, the average crystallite size was found to be in the range of 34-39 nm (Table 1). The estimated value of crystallite size was decreased by the effect of Sr^{2+}. Considering the ionic radius, for Sr^{2+} (0.113 Å) it is greater than that of the Ca^{2+} (0.99 Å). It is expected that the incorporation of Sr might cause the shrinkage (size reduction) of the apatitic structure [16].

While the crystallinity (X_c) of the as-synthesized nanoparticles [17] was calculated from the following Equation [3],

$$X_c = \left(\frac{0.24}{\beta}\right)^3 \quad [3]$$

The average crystallinity on Sr substituted HA sample was similar to that of crystallite size calculated. The decreased crystallinity and crystallite size of Sr incorporated HA samples were further confirmed by FESEM results. In order to keep charge compensation mechanism, the vacancies and defects are generated and this would affect the crystallinity [8].

The lattice parameters a and c for the obtained hexagonal structure were calculated from (211) and (002) planes respectively using the following relation

$$\frac{1}{d^2_{(hkl)}} = \frac{4}{3}\left(\frac{h^2 + hk + k^2}{a^2}\right) + \frac{l^2}{c^2} \qquad [4]$$

The lattice parameters of pure HA varied with small amount of strontium. In the case, both ions Sr^{2+} and Ca^{2+} have similar charges but the size difference may linked with an expansion of apatite lattice parameters. The slight change of the lattice parameters of Sr-HA clearly revealed the Sr ions were structurally incorporated into HA lattice. Moreover, Stokes-Wilson equation was used to determine the lattice strain (Ɛ)

$$\varepsilon = \frac{\beta}{4\tan\theta} \qquad [5]$$

There is a broadening observed at FWHM of the XRD pattern with inclusion of Sr^{2+}. This broadening is caused by not only the crystalline size-induced but also to the strain-induced broadening. The influence of lattice strain values on the XRD peak reflection is clear from the Table 1.

3.2. FTIR analysis

The functional group analysis of pure and Sr-substituted HA nanoparticles confirmed the fundamental vibration bands corresponding to hydroxyapatite as shown in Fig. 2. The bands associated with different characteristic vibration modes around 466, 568, 606, 976 and 1030-1100 cm^{-1} demonstrates the PO_4 groups of the apatite structure [18]. The absorption band at 3442 cm^{-1} and 1695 cm^{-1} correspond to absorbed water. The strongest band at 1037-1100 cm^{-1}, which appears as a doublet in Sr substituted HA sample was assigned to the phosphate stretching vibration. The weak band at about 453 cm^{-1} associated to the phosphate banding mode. The band at 568-606 cm^{-1} appears as a doublet was assigned to the PO_4^{3-} bending modes [19]. The weak vibrational peak at 1448 cm^{-1} is attributed to the presence of carbon moieties on pure HA sample formed during the stage of sample preparation.

Table 1 The average crystallite size and crystallinity values for synthesized HA samples

Sample	Chemical formula	Crystallite size (D) (nm)	Crystallinity (X_C)	Lattice Parameter (Å)		Strain (ε) x 10^{-3}
				a	b	
Pure HA	$Ca_{10}(PO_4)_6(OH)_2$	38.82	1.7401	9.4261	6.7762	0.2232
Sr-HA	$Ca_{0.95}Sr_{0.05}(PO_4)_6(OH)_2$	33.42	1.3040	9.4422	6.8102	0.2725

3.3. Morphological analysis

FESEM micrographs of the synthesized pure HA and Sr-substituted HA nanoparticles are exhibited in Fig.3. The surface morphology of pure HA nanoparticles show spherical shaped morphology (Fig.3 (a)) with average diameter ranging from 70 to 86 nm. Micrographs revealed that Sr ions doping influenced the particle size of the HA nanoparticles (Fig.3 (b)). In Sr- HA sample, formation of spherical shaped with loosely agglomeration of primary particles with averages diameter ranging below 70 nm. The agglomeration of both samples consisting of interconnected elongated spherical-like particles. The decrease in the size of HA nanoparticles was also confirmed by XRD analysis as shown in Table 1.

3.4. Dielectric and AC conductivity

The dielectric possession of the material plays a vital role in various areas of science and engineering. The real part of dielectric permittivity, Ɛ′ attributed to the dielectric constant and the imaginary part Ɛ″, the dielectric loss, and the AC conductivity (σ_{ac}) are calculated by the following relations [14]

$$\varepsilon^* = \varepsilon' - i\varepsilon'' \quad (6)$$

$$\varepsilon' = \frac{C_p\, t}{\varepsilon_0 A} \quad (7)$$

$$\varepsilon'' = \frac{G_c\, t}{\varepsilon_0 A \omega} \quad (8)$$

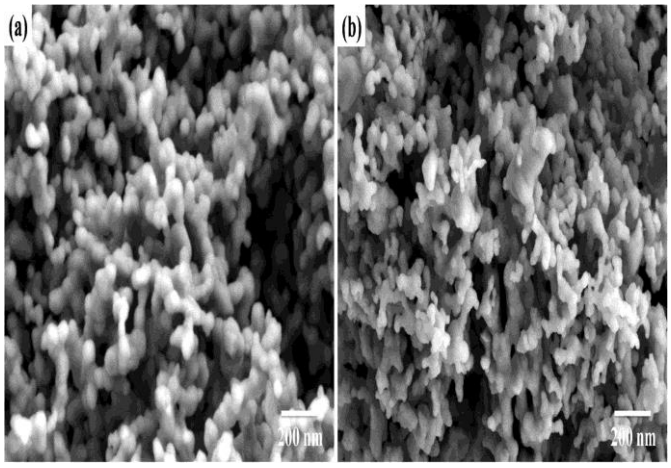

Fig .3. FESEM micrograph of (a) pure and (b) Sr2+-substituted HA nanoparticles.

$$\sigma_{ac} = 2\pi f \varepsilon_0 \varepsilon' \tan\delta \quad (9)$$

Where ε_0 is the permittivity of free space charge (ε_0=8.854 x10^{-14} F/cm), A is the area of the electrode, t is thickness of the sample, tanδ is the tangent loss factor (tanδ=ε"/ ε'), C_p and G_c are the capacitance and conductance, and f is frequency of

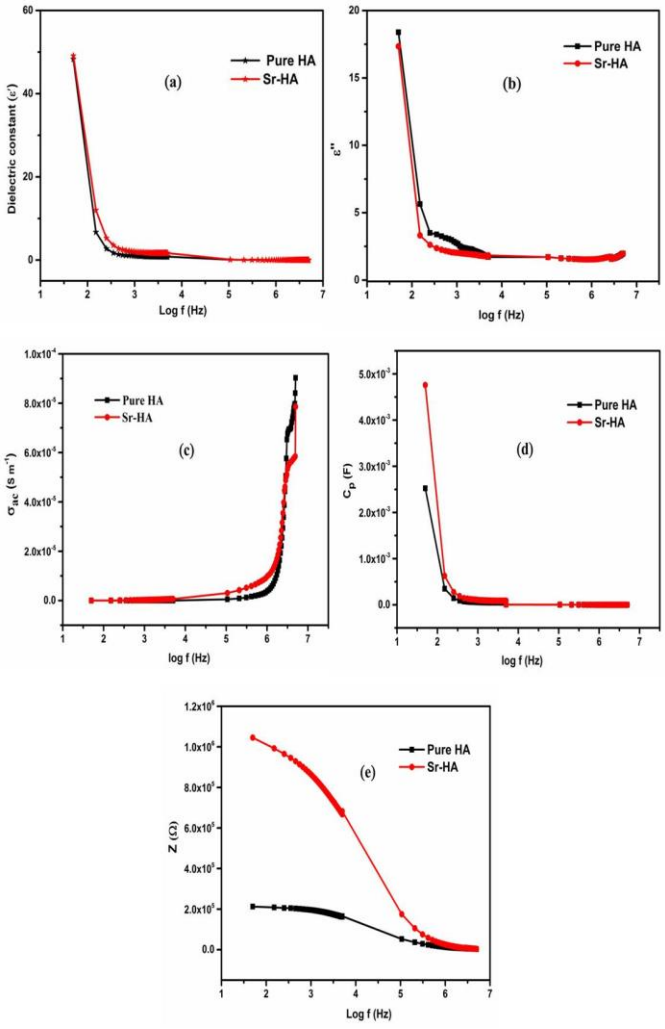

applied ac field and $\omega = 2\pi f$ is the angular Fig. frequency respectively.

Fig 4. The frequency variation of (a) dielectric constant (ε'), (b) dielectric loss (ε''), (c) Ac conductivity (σ_{ac}), (d) capacitance (C_p) and (e) Impedance.

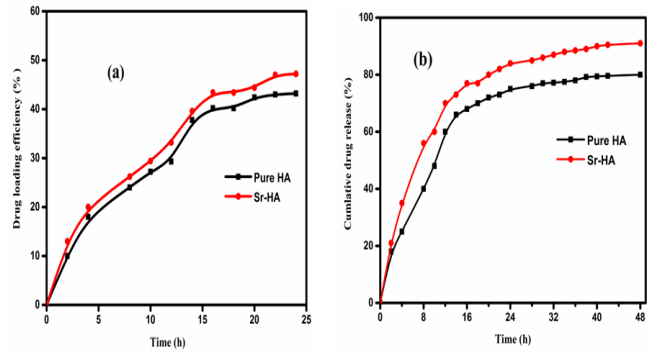

Fig. 5.*In vitro* amoxicillin drug loading and release of pure and Sr-HA as a function of time.

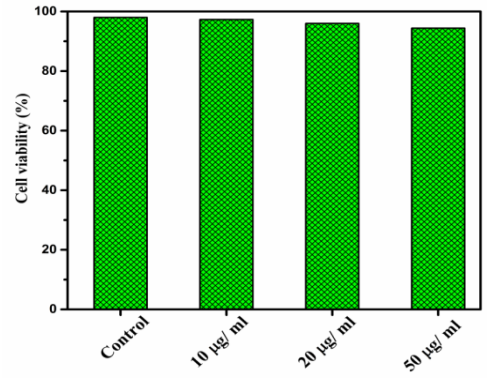

Fig.6. The Cell viability of A549 cells against Sr-HA Nanoceramics at different concentrations.

The dielectric permittivity (Ɛ′) dependence on applied frequency of the as-synthesized HA nanoparticles are shown in Fig. 4 (a). The change in the dielectric constant of both pure and Sr-HA sample is due to the electrical polarization. The incorporation of Sr into Ca ion in HA changes the dielectric dipole moments of the hydroxyl ions having an ionic structure are oscillated with the frequency of applied electric field [20]. The change in oscillations of dipoles causes a change in the dielectric constant. The dielectric loss (Ɛ″) established using Eq. 8, also gradually decreases with increasing the frequency and inclusion of strontium ions as shown in Fig. 4 (b). The reduction of dielectric loss (Ɛ″) at low frequencies is attributed to the migration of ions in the HA samples.

Fig 4(c) shows that the ac conductivity (σ_{ac}) gradually increases with frequency from 50 Hz to 5MHz at room temperature for HA and Sr-HA samples and obeys the universal power law. However the conductivity mechanism of the samples is confirmed by using the well-known Jonscher relation [21]:

$$\sigma_{ac} = \sigma_{dc} + B\omega^{s} \qquad (10)$$

Where σ_{dc} is the direct current conductivity, B is a constant, ω is the angular frequency, and s is an exponent. In this regard, pure HA and Sr substituted HA samples exhibit the conductivity mechanism, which was in good agreement with the previous results [22, 23]. The capacitance and impedance values decrease with frequency (Fig. 4 d &e), but the values of the ac conductivity increase. The capacitance decays for all the samples in the high-frequency region that follow the conductivity [14]. The measured resistance values range from 10^5-$10^6\Omega$, and this value corresponds to insulator behavior of pure and Sr substituted HA the samples.

3.5. In Vitro drug loading and release

The UV-vis demonstrates that amount of doxycycline drug loading efficiency of pure and Sr-substituted HA nanoparticles corresponding with time are shown in Fig.5 (a). This result interesting to note that loading and prolonged realise of drug has been observed for both samples. Nevertheless, the percentage of drug loading was Found to be 43.1% for pure HA and 46.1% for $Sr_{0.1}HA$ samples. Doxycycline have easily water soluble drug and contains electron-donor groups likely to generate stable complexes with Ca^{2+} and Sr^{2+} thus presenting a strong affinity for the adsorption on HA surface [24].

The amounts of drug release from pure HA, and Sr-HA was shown in Fig. 5 (b). It revealed that the release of amoxicillin drug from the Sr substituted HA was relatively faster than pure HA samples. An initial burst release of about 40 % within 7- 8 h for both samples, after the rapid release stage followed by the prolonged release. While the rate of drug release attained at maximum for both samples time takes over 48 h. The initial stage of rapid drug release may be attributed to the adsorption of drugs on the outer surface of samples [15, 25]. The slow release may response to the high affinity between drug molecules and the inner apatite surface. It is interesting to note that the as-synthesized HA nanoparticles can exhibit sustained and prolonged release for the promising application of drug vehicle in targeted sites.

3.6. Cell viability in vitro

The MTT assay is a convenient approach to find the cell viability of bioceramic materials. The in vitro cytotoxicity of Sr substituted HA was evaluated by MTT assay against human lung carcinoma epithelial-A549 cell line, and pure HA was used as a control as shown in Fig. 6. The cells exposed to the samples different concentration (10, 25 and 50 µg mL^{-1}) shows no remarkable changes in the MTT signal as compared to control. The cell viabilities are all over 90 %, and the sample Sr substituted HA is exhibited better biocompatibility. Therefore, free toxicity of Sr-HA biomaterials can be potential candidate for various biomedical applications.

4. Conclusions

In summary, pure and Sr substituted HA nanoparticles were successfully synthesized by sol-gel method and their structural and electrical properties were also investigated. The inclusion of Sr ions in the apatite structure could influence on pure HA properties, by reducing their crystallite size, crystallinity good harmony with the

morphology analysis. Functional group analysis from the FT-IR spectra confirmed the formation of HA due to the presence of hydroxyl and phosphate groups in both samples. The relative permittivity, dielectric loss and alternating current conductivity changes with increasing frequency and the ac conductivity (σ_{ac}) increased with an increasing applied frequency confirmed that HA sample exhibited the universal power law nature. The Sr^{2+} substituted HA sample showed extended drug release and exhibited better biocompatibility. Hence, thus bioceramics can be potential candidate for various biomedical and optoelectronic applications.

Reference

[1] Shuyun Qi, Yanlin Huang, Yadong Li, PeiqingCai, Sun ll Kim and Hyo Jin Seo, Probe spectrum measurements of Eu^{3+} ions as a relevant tool for monitoring *in vitro* hydroxyapatite formation in a new borate biomaterial,*J. Mater. Chem. B* 2 (2014) 6387-6396.

[2] Ruixue Sun, Kezheng Chen, Xiangfeng Wu, Dandan Zhao and Zhenzong Sun, Controlled synthesis and enhanced luminescence of europium-doped fluorine-substituted hydroxyapatite nanoparticles,*Cryst. Eng. Comm.* 15 (2013) 3442-3447.

[3] Sophie C. Cox, ParastooJamshidi, Liam M. Grover andKajal K. Mallick, Preparation and characterisation of nanophaseSr, Mg, and Zn substituted hydroxyapatite by aqueous precipitation, *Mater. Sci. Eng C* 35 (2014) 106-114.

[4] D. Gopi, S. Nithiya, E. Shinyjoy and L. Kavitha. Spectroscopic investigation on formation and growth of mineralized nanohydroxyapatite for bone tissue engineering applications, *Spectrochim. Acta. Part A.* 92(2012)194-200.

[5] Omer Kaygili, SerhatKeser, Mustafa Kom, YesariEroksuz, Sergey V. Dorozhkin andTankutAtes, Strontium substituted hydroxyapatites: Synthesis and determination of their structural properties, *in vitro* and *in vivo* performance,*Mater. Sci. Eng C.* 55 (2015) 538-546.

[6] LakshmanaperumalSundarabharathi, MahendranChinnaswamy, DeepalekshmiPonnamma, HemalathaParangusan and Mariam Al Ali Al-Maadeed, Investigation of Antimicrobial Properties and *in-vitro* Bioactivity of Ce^{3+}-Sr^{2+}Dual-substituted nano Hydroxyapatites,*J. Am. Ceram. Soc.*102 (2018) 144-157.

[7] S. Hesaraki, M. Alizadeh, H. Nazarian and D. Sharifi, Physico-chemical and in vitro biological evaluation of strontium/calcium silicophosphate glass, *J. Mater. Sci. Mater. Med.* 21 (2010) 695-705.

[8] S. Lakshmanaperumal, P. Hemalatha, D. Ponnamma and C. Mahendran, In-vitro biocompatibility, bioactivity and photoluminescence properties of Eu3+/Sr2+ dual-doped nano-hydroxyapatite for biomedical Applications,*J. Biomed. Mater. Res. B*, 106 (2018) 2191-2201.

[9] Matteo Frasnelli1, Francesco Cristofaro and Vincenzo M. Sglavo, Synthesis and characterization of strontium-substituted hydroxyapatite nanoparticles for bone regeneration,*Mater. Sci. Eng. C 71* (2017) 653-662

[10] R.V.Suganthi, K.Elayaraja, M.I.AhymahJoshy, C.V.Sarath, E.K.Girija and S.NarayanaKalkura, Fibrous Growth of Strontium substituted hydroxyapatite and its drug release, Mater.Sci. Eng. C 31(2011) 593-599.

[11] V.H. Pham andN.N. Trung, Luminescence of europium doped silicon-substituted hydroxyapatite nanobiophosphor via a co-precipitation method,*Mater. Lett.* 136 (2014) 359-361.

[12] L.M. Silva, D.S. Menezes andL.E. Almeidaa, The role of the counter-ions present in syntheses on the thermal stabilization of strontium and/or calcium apatites,*Mater. Sci. Eng. B* 199 (2015) 77-86.

[13] N. Iqbal, M.R.A. Kadir, N.A.N.N. Malek, N.H. Mahmood, M.R. Murali andT.K. Zama, Rapid microwave assisted synthesis and characterization of nanosized silver-doped hydroxyapatite with antibacterial properties,*Mater. Lett.* 89 (2012)118-122.

[14] S. Lakshmanaperumal and C. Mahendran, Structural, dielectric, cytocompatibility, and *in vitro* bioactivitystudies of yttrium and strontium co-substituted nanohydroxyapatite by sol–gel method, J. Sol-Gel SciTechn,88 (2018) 296-308.

[15] M.I. AhymahJoshy, K. Elayaraja, R.V. Suganthi, Sarath Chandra Veerla and S. NarayanaKalkura, *In vitro* sustained release of amoxicillin from lanthanum hydroxyapatite nano rods, CurrAppl Phys. 11 (2011) 1100-1106.

[16] O. Kaygili, S.V. Dorozhkin,T. Ates, N.C. Gursoy, S. Keser, F. Yakuphanoglu andA.B. Selçuk, Structural and dielectric properties of Yttrium-substituted Hydroxyapatites, *Mat. Sci. Eng. C* 47 (2015)333-338.

[17] E.Landi, A. Tampieri, G. Celotti and S. Sprio, Densification behaviour and mechanisms of synthetic hydroxyapatites, *J. Eur. Ceram. Soc.,* 20 (2000) 2377–2387.

[18] D. Fabio Mercado, GiulianaMagnacca, MeryMalandrino, Aldo Rubert, EnzoMontoneri andLuisellaCeli, Paramagnetic Iron-Doped Hydroxyapatite Nanoparticles with Improved Metal Sorption Properties A Bioorganic Substrates-Mediated Synthesis, *ACS Appl. Mater. Interfaces* 6 (2014) 3937−3946.

[19] V.Stanic, D.Janackovic, S.Dimitrijevic, S.B.Tanaskovic, M. Mitric and M.S.Pavlovic, Synthesis of antimicrobial monophase silver doped hydroxyapatite nanoparticles for

bone tissue engineering, *Appl. Sci.* 257 (2011) 4510-4518.

[20] Faten E. Al-Hazmi, Synthesis and electrical properties of Bi doped hydroxyapatite Ceramics, *J. Alloy. Compd.*665 (2016) 119-123.

[21] A.K. Jonscher, The universal dielectric response,*Nature* 267 (1977) 673-679.

[22] O. Kaygili, T. Ates, S. Keser, A.A. Al-Ghamdiand F. Yakuphanoglu, Controlling of dielectrical properties of hydroxyapatite by ethylenediaminetetraacetic acid (EDTA) for bone healing applications,Spectrochim. Acta A, 129 (2014) 268-273.

[23] O. Kaygili, S.V. Dorozhkin, T. Ates, A.A. Al-Ghamdi andF. Yakuphanoglu, Dielectric properties of Fe doped hydroxyapatite prepared by sol-gel method,*Ceram Int.* 40 (2014) 9395-9402.

[24] S. Wang, X. Wang, H. Xu, H. Abe, Z.Tan, Y. Zhao, J. Guo, M.Naito, H. Ichikawa and Y. Fukumori, Towards sustained delivery of small molecular drugs using hydroxyapatite micro spheres as the vehicle, *Adv Powder Technol.*21(2010) 268–272.

[25] P. Yang, Z. Quan, C. Li, X. Kang, H. Lian and J. Lin, Bioactive, luminescent and mesoporous Europium -doped hydroxyapatite as a drug carrier, *Biomaterials.* 29 (2008) 434-437.

About The License